Holey Reduced Graphene Oxide Scaffolded Heterocyclic Aramid Fibers with Enhanced Mechanical Performance

Jiaqiang Li, Yeye Wen, Zhihua Xiao, Shijun Wang, Lixiang Zhong, Tao Li, Kun Jiao, Lanying Li, Jiajun Luo, Zhenfei Gao, Shuzhou Li, Zhong Zhang,* and Jin Zhang**

Dr. J. Q. Li, Dr. Y. Y. Wen, Dr. Z. H. Xiao, Prof. K. Jiao, J. J. Luo, and Prof. J. Zhang
Center of Nano Chemistry, Beijing National Laboratory for Molecular Sciences, College of Chemistry and Molecular Engineering, Peking University, Beijing 100871, China.
E-mail: jinzhang@pku.edu.cn

Dr. J. Q. Li, Dr. Y. Y. Wen, Dr. Z. H. Xiao, Dr. T. Li, Prof. K. Jiao, J. J. Luo, Prof. Z. F. Gao, and Prof. J. Zhang
Beijing Graphene Institute (BGI), Beijing 100095, China

Prof. K. Jiao, L. Y. Li and Prof. J. Zhang
School of Materials Science and Engineering, Peking University, Beijing 100871, China

Dr. S. J. Wang and Prof. Z. Zhang
National Center for Nanoscience and Technology, Beijing 100190, China
E-mail: zhongzhang@ustc.edu.cn

Dr. L. X. Zhong and Prof. S. Z. Li
School of Materials Science and Engineering, Nanyang Technological University, Singapore 639798, Singapore.
E-mail: LISZ@ntu.edu.sg

Prof. Z. Zhang
CAS Key Laboratory of Mechanical Behavior and Design of Materials, Department of Modern Mechanics, University of Science and Technology of China, Hefei 230026, China

Dr. T. Li
Faculty of Materials and Manufacturing, Beijing University of Technology, Beijing 100021, China

L. Y. Li
China Bluestar Chengrand Chemical Co. Ltd, Chengdu 610041, China

Dr. J. Q. Li
Advanced Membranes and Porous Materials Center, Physical Sciences and Engineering Division, King Abdullah University of Science and Technology, Thuwal 23955-6900, Saudi Arabia.

Keywords: holey graphene, heterocyclic aramid fibers, scaffolded structure, lateral interaction, mechanical properties

Abstract: Poly(p-phenylene-benzimidazole-terephthalamide) (PBIA) fibers, a kind of heterocyclic aramid fibers, possess extraordinary mechanical properties and advanced applications in aerospace, military protection, and other civilian areas. However, harsh application scenarios are putting forward even stringent requirements for the mechanical performances and environmental compatibility of PBIA fibers. Strengthening lateral interactions between polymer chains are approachable methods but ongoing challenges to obtain PBIA fibers with high-performance. This work develops a novel holey reduced-graphene-oxide (HrGO)/PBIA composite fiber with a scaffolded structure, in which the HrGO plays a role of clamp to effectively band plentiful PBIA chains through the in-plane holes. A small amount of HrGO (0.075 wt%) is able to improve the tensile strength and Young's modulus of HrGO/PBIA fibers by 11.5 and 8.3%, respectively. The small amount of well dispersed HrGO improves the crystallinity and serves as the topological constraint that enhances the lateral interaction of the PBIA chains, which is unveiled by the wide-angle X-ray scattering and the coarse-grained molecular dynamics simulations. In addition, the favorable compatibility of HrGO/PBIA fibers in complex application scenarios is demonstrated by the dynamic and cyclic-loading measurements.

Introduction

Aramid fibers are typical high-performance organic fibers[1-2] possessing splendid mechanical properties and comprehensive applications in advanced fields, such as aerospace,[3] military protection and other civilian areas.[4-5] Especially, poly(p-phenylene-benzimidazole-terephthalamide) (PBIA) fibers, a kind of heterocyclic aramid (HA) fibers that introduce asymmetric heterocyclic units 2-(4-aminophenyl)-5-aminobenzimidazole (PABZ) into the poly(p-phenylene-terephthalamide) (PPTA) main chains,[6-8] present superior comprehensive performance than other aramid fibers due to their special chemical structures.[6, 9] Since Kamenskvolokno (Russia) first synthesized PBIA fibers (SVM) in 1970s, several versions of PBIA fibers have been developed subsequently.[9] The upgrading of products is accompanied by continuous improvement in performances, leading to rapid development of preparation technologies. However, current tensile strength (4.5-5.5 GPa) and Young's modulus (140.0-146.0 GPa) of PBIA fibers still have a large gap with the theoretical predications (tensile strength larger than 30.0 GPa and modulus larger than 182.0 GPa) due to the inevitable structural defects (such as voids and ends of chains) in fibers and weak lateral interactions between polymer chains.[10-12] Meanwhile, harsh application scenarios of PBIA fibers are putting forward even stringent requirements for their mechanical performances and environmental compatibility.[13] Therefore, many efforts have been devoted to improving the mechanical properties of PBIA fibers. Besides the optimization on polymerization and spinning processes for increasing the crystallinity and orientation degree,[13-14] enhancing lateral interactions between polymer chains are approachable methods by introducing inter-chain hydrogen or covalent bonding.[15] However, additionally introducing hydrogen bonding interaction is limited since pristine PIBA fibers have been equipped with ample hydrogen bonds between polymer chains.[16-17] Although strong inter-chain interaction based on chemical crosslinking can increase the shear strength between polymer chains and has pronounced effect on the enhancement of compressive strength of fibers,[18-21] the reducing crystallinity and orientation degree of fibers

lead to restricted improvement of tensile strength, even deteriorating strength sometimes.[18] Thus, realizing the effective stress transfer between polymer chains without sacrificing structural integrity of PBIA fibers is an ongoing challenge.

Because of the extraordinary mechanical properties (130.0 GPa of tensile strength and 1.0 TPa of Young's modulus) and huge specific surface area,[22-27] graphene has long been considered as an efficient reinforcement for composite polymer materials with high performance and advanced functions.[28-29] In particular, graphene and graphene oxide (GO) have been adopted to strengthen the lateral interaction of polymer chains in aramid fibers through π-π interaction, leading to improvement in tensile strength and modulus.[22, 30] However, these strategies present limited effects for improving mechanical performances because of the weak and noncovalent lateral interactions. Moreover, the interaction sites are limited across the radial direction of fibers in low concentration of graphene since the interaction only exists between graphene and the adjacent polymer chains (Figure S1a). Improving the loading amount of graphene are helpful but restricted by the dispersion related issues of graphene. Therefore, developing an effective composite way to fully utilize the properties of graphene is essential for preparing graphene-reinforced PBIA fibers.[30]

Inspired by the structure of scaffold which is made up with tubes and clamps (Figure S1b) and the unique two-dimensional (2D) structure of graphene, we developed an *in-situ* polymerization method to build a scaffolded structure consisting of holey reduced graphene oxide (HrGO) and PBIA macromolecular chains, in which the PBIA chains (Tubes) run through the holes of HrGO (Clamps) to form a robust topological constraint structure (Figure S1c). Different from the graphene or rGO, HrGO can provide more lateral contacting sites with polymer chains. Besides the intrinsic hydrogen bonding and π-π interaction between polymer chains of PBIA fibers, the HrGO plays a role of clamp to effectively band plentiful polymer chains through the in-plane holes, promoting sufficient stress transfer between polymer chains across radial direction of fibers. As a result, a small amount of HrGO can enhance the mechanical properties of the

HrGO/PBIA fibers. Typically, HrGO/PBIA fibers with 0.075 wt % HrGO exhibit a tensile strength of 5.81 GPa and Young's modulus of 134.2 GPa, which represent a 11.5% increasement in strength and 8.3% increasement in Young's modulus compared with those of pure PBIA fibers. Dynamic experiments results reveal that HrGO/PBIA fibers exhibits better mechanical properties than PBIA fibers under different loading frequencies and strain rates, indicating HrGO/PBIA fibers would present excellent compatibility under complicated and volatile application scenarios. Coarse-grained model simulations jointly elucidated the microstructure modification and enhancement mechanism of HrGO/PBIA fibers. These insights not only expand the understanding of PBIA fibers but also provide a novel preparation method for graphene-reinforced composite fibers.

Results and discussion

In this work, the polymer chain of PBIA fibers is a copolymerized production from three monomers (Scheme S1): *p*-phenylenediamine (PPD), terephthalyl chloride (TPC), and PABZ. The schematic preparation of HrGO/PBIA composite spinning dope and HrGO/PBIA fibers is depicted in **Figure 1**a. Firstly, the HrGO was prepared by heating a homogeneous aqueous mixture of GO and H_2O_2 (Figure S2).[31] Then, *in-situ* polymerization was conducted in dimethylacetamide (DMAC) with 3.5 wt% lithium chloride (LiCl) in the presence of HrGO and monomers of PBIA. The amidation reaction of monomers produced PBIA chains which would run through the holes on HrGO to form a scaffolded structure. Then, wet-spinning technologies were employed to process the HrGO/PBIA composite spinning dope to obtain HrGO/PBIA fibers. The detail preparation processes are shown in Figure S3. In order to understand the monomer polymerization in the holes of HrGO, the density functional theory (DFT) calculations were performed to investigate the potential energies for the polymerization of TPC and PPD in different adsorption configurations. Figure 1b displays the potential energies of amidation of PPD and TPC in the absence of HrGO. The rate-determining step is the

dehydrogenation process which has a very low energy barriers of 0.053 eV (Figure S4a), indicating the amidation process is a spontaneous reaction. Then HrGOs with different hole diameters (from 0.54 to 1.27 nm) were introduced into the reaction system to investigate the potential energies of PPD and TPC reacting in the hole (Figure S4b-e). The energy barrier of polymerization in the hole with a diameter about 0.54 nm is 3.16 eV which is much larger than that in solution (Figure S4b). The high reaction barrier is resulted from the strong intermolecular repulsion which will hinder the amidation of PPD and TPC, indicating that PPD and TPC tend to polymerize in solution rather than in the holes of HrGO. A very low energy barrier (0.028 eV) of corresponding step was obtained when the hole diameter was extended to 1.27 nm (Figure S4d), even though the HrGO with hydroxyls in the margin of holes (Figure 1c). These results indicate that the PIBA polymer chain will run through the holes of HrGO without boundaries when the hole diameter on HrGO is larger than 1.27 nm.

The structure of HrGO and practical scaffolded structure of HrGO/PBIA fibers were considered. **Figure 2**a displays the atomic force microscopy (AFM) image of HrGO, the thickness of HrGO is about 0.7 nm, corresponding to monoatomic thickness. Figure 2b displays the scanning electron microscopy (SEM) image of HrGO. The average lateral size of HrGO is about 1.36 μm with a narrow distribution centered at 1-2 μm (inset of Figure 2b). Deoxygenation was observed in the narrow X-ray photoelectron spectroscopy (XPS) and Fourier-transform infrared spectroscopy (FT-IR) spectra of GO and HrGO (Figure S5), indicating the HrGO is partial reduced compared to pristine GO.[31] The Raman spectrum of HrGO shows an increased intensity ratio of D to G band (1.05) in comparison with GO (0.95) (Figure S6a), ascribing to the solvent-assisted thermal reduction. Nitrogen adsorption−desorption characterizations show the HrGO exhibits a much higher Brunauer–Emmett–Teller (BET) specific surface area (~299.1 $m^2 g^{-1}$) than GO (~263.6 $m^2 g^{-1}$) (Figure S6b). A larger hysteresis loop is observed in the BET curve of HrGO compared with that of GO, suggesting that the HrGO endows abundant mesopores. Transmission electron microscopy (TEM) and SEM images further reveal the abundant in-plane

holes across HrGO (Figure 2c,d) which is clearly contrast to hole-free rGO sheets prepared using the same procedures as HrGO without using H_2O_2 (Figure S6c,d). Statistical hole size of HrGO treated by H_2O_2 for 8 h exhibits a pore size distribution in the range of 5−20 nm (inset of Figure 2c) which is much larger than aforementioned critical hole dimeter (1.27 nm) from DFT results, indicating monomers of PBIA can readily polymerize in the holes of HrGO. Smaller lateral size (1-3 nm) of HrGO will be obtained while reacting with H_2O_2 for 4 h (Figure S7). In order to confirm the scaffolded structure of HrGO/PBIA fibers, SEM and TEM characterizations were utilized to disclose the microstructure of HrGO/PBIA by dissolving composite fibers in KOH/dimethyl sulfoxide (DMSO)/DMAC solution.[32] As shown in Figure 2e, PBIA chains and HrGO are observed in the SEM image of HrGO/PBIA composite and the HrGO is intersected with several PBIA chains. The scaffolded structure of HrGO/PBIA was further demonstrated by the TEM image (Figure 2f), in which a linear PBIA chain running through a hole of HrGO is observed clearly.

HrGO/PBIA composite fibers with different HrGO concentrations (from 0 wt% to 0.3 wt%) and rGO/PBIA fibers were prepared through a lab-made wet-spinning system. The favorable dispersibility of HrGO was confirmed by a homogeneous HrGO dispersion (1.8 mg mL^{-1}) in DMAC after a quiescence for 48 h and the particle size analyze results indicate that particle size of HrGO in DMAC is about 1.52 μm (Figure S8), which agrees with the lateral size investigation from SEM results (Figure 2b). **Figure 3**a,b display the SEM images of HrGO/PBIA fibers with an HrGO concentration of 0.075 wt% (0.075-HrGO/PBIA) and PBIA fibers. Both 0.075-HrGO/PBIA and PBIA fibers clearly display smooth surface and diameters about 14.91 and 15.35 μm (top-right insets of Figure 3a,b), respectively. The uniform dispersion of HrGO also endows 0.075-HrGO/PBIA fibers with a darker color than PBIA fibers (top-left insets of Figure 3a,b). Cross-section SEM images reveal that 0.075-HrGO/PBIA fibers (Figure 3c) have a very tight structure in the lateral direction of fibers as PBIA fibers (Figure 3d), indicating a good dispersibility of HrGO in 0.075-HrGO/PBIA fibers. SEM images of

HrGO/PBIA fibers containing 0.01 wt%, 0.025 wt%, and 0.05 wt% HrGO (0.01-HrGO/PBIA, 0.025-HrGO/PBIA, and 0.05-HrGO/PBIA) show that all the fibers have smooth surface as 0.075-HrGO/PBIA (Figure S9a-c). The surface of fibers becomes rough while the concentration of HrGO is up to 0.1 wt% (Figure S9e). Moreover, obvious broken filaments are observed in 0.3-HrGO/PBIA fibers (Figure S9f). Cross-section SEM images further display the existence of voids in 0.1-HrGO/PBIA and 0.3-HrGO/PBIA fibers (Figure S10). These results indicate that a high concentration of HrGO would result in the incompact structures and increase the defect density of the composite fibers because of the aggregation of HrGO.

FT-IR spectra of PBIA, 0.075-HrGO/PBIA, and 0.075-rGO/PBIA fibers are shown in Figure 3e. All the spectra display characteristic amide absorption bands. The absorption band at about 1635 cm^{-1} is assigned to the C=O stretching vibrations in the amide groups. The bands at 1610, 1247, and 1310 cm^{-1} are assigned to the C=N, N-H, and C-N vibrations of the benzimidazole group, respectively, indicating the successful introduction of PABZ units in HrGO/PBIA fibers. These absorption bands are characteristics for PBIA and are consistent with the previous work.[33] There are not obvious differences in the vibration of carbon-carbon double bonds in PBIA and HrGO/PBIA fibers since the loading amount of HrGO is very low. FT-IR spectra of HrGO/PBIA fibers with different HrGO concentrations are displayed in Figure S11 which present similar result as PBIA fibers. Thermal properties of the PBIA, 0.075-HrGO/PBIA, and 0.075-rGO/PBIA fibers were evaluated by thermogravimetric analysis (TGA) in oxygen atmosphere as shown in Figure 3f. Obviously, PBIA fibers exhibit a main decomposition temperature ranging from 510 to 610 ºC at a heating rate of 10 ºC min^{-1}. 0.075-HrGO/PBIA fibers present higher decomposition temperature and larger residual mass comparing with PBIA and 0.075-rGO/PBIA fibers, indicating HrGO/PBIA fibers possess favorable thermostability and oxidation-resistance. The one-dimensional (1D) wide-angle X-ray scattering (WAXS) profiles of PBIA, 0.075-HrGO/PBIA, and 0.075-rGO/PBIA fibers are shown in Figure 3g and display four obvious peaks at 2θ = 14.19º, 20.26º, 28.32º, and 43.82º.[7] All the scattering peaks

of 0.075-rGO/PBIA exhibit narrower full width at half maxima of peaks than that of PBIA, indicating that 0.075-rGO/PBIA fibers possess higher crystallinity than PBIA fibers. The introduced rGO can serve as both the template for the alignment and orientation of polymer chain and the nucleating agent for the polymer crystallization.[25] The scattering peaks of 0.075-HrGO/PBIA are narrower than that of 0.075-rGO/PBIA, which indicates the further improved crystallinity of 0.075-HrGO/PBIA fibers compared to 0.075-rGO/PBIA, demonstrating that the topological constraint effect in 0.075-HrGO/PBIA is beneficial to crystallization of polymer chains. 2D WAXS was further applied to characterize the orientation of PBIA, 0.075-HrGO/PBIA, and 0.075-rGO/PBIA fibers and the corresponding results are shown in Figure 3h-j. The scattering halo of PBIA fibers exhibits a slight reinforcement on the equator (Figure 3h) in the 2D-WAXS pattern, indicating an ordered intermolecular packing in the transverse fiber direction.[6] And there are not diffraction spots but broad diffraction rings along the meridian. After introducing 0.075 wt% HrGO and rGO, the diffraction spots on the equator become stronger and narrower than that of PBIA fibers and obvious diffraction spots along the meridian were observed (Figure 3i,j) in the 2D-WAXS pattern of 0.075-HrGO/PBIA and 0.075-rGO/PBIA fibers, indicating the improvement of orientation of 0.075-HrGO/PBIA and 0.075-rGO/PBIA fibers compared to PBIA fibers.

The results of mechanical properties measurements demonstrate that introducing HrGO into the PBIA can improve the mechanical performance of the resultant composite fibers. After evaluating the tensile strength and Young's modulus of HrGO/PBIA fibers with HrGO concentrations from 0.025 to 0.3 wt% (**Figure 4**a), gradual strengths increasing are observed when the HrGO concentrations increase from 0.025 to 0.075 wt% and HrGO/PBIA fibers exhibit reduced tensile strength when HrGO concentration is larger than 0.1 wt%. Notably, 0.075-HrGO/PBIA fibers present the highest strength (5.81 GPa) and modulus (143.2 GPa) among these investigated composite fibers. Despite of the small value of mass fraction (0.075 wt%), the effective volume, on which the HrGO exerts topological confinements, can be up to

18 vol% of the total fiber due to the large aspect ratio of HrGO (Figure S12). Specifically, we estimate the effective volume by assuming that each HrGO is able to confine the volume of fiber within its radius and the HrGO is uniformly dispersed. The exploit of the HrGO not only introduces the topological confinements in the lateral direction, which restrict the slippage, reorientation and motion of polymer chains,[34] but also optimize the arrangement of crystalline and amorphous regimes.[35] The deteriorated mechanical properties of HrGO/PBIA fibers with the exceeding HrGO concentration are attributed to the aggregation of HrGO, which will affect the polymerization of PBIA monomers and reduce the orientation of PBIA polymer chains, as well as lead to the voids accumulating in composite fibers.[12] Similar results have been reported for carbon nanotubes and other graphene reinforced polymer composites.[25, 36] Figure 4b displays the tensile strength and modulus of PBIA, 0.075-HrGO/PBIA, and 0.075-rGO/PBIA fibers. The strength and modulus of 0.075-HrGO/PBIA are 11.5 and 8.3% larger than those of PBIA fibers, respectively. 0.075-rGO/PBIA fibers present the lower tensile strength (5.28 GPa) and modulus (124.3 GPa) than those of 0.075-HrGO/PBIA fibers. Based on the molecular weight results, the HrGO/PBIA and rGO/PBIA fibers present higher average molecular weight than PBIA fibers (Figure S13). The increased molecular weight could be attributed to the interaction of PIBA polymers and fundtional groups of HrGO/rGO which would improve mechanical strength and stability to a certain extent. However, the tensile strength of HrGO/PBIA fibers exhibit a greater improving degree than that of rGO/PBIA fibers (11.5 % *vs.* 1.3 %). Therefore, the enhanced mechanical properties of HrGO/PBIA fibers would mainly derive from the key role of holes in HrGO rather than the functional groups. 0.075-HrGO/PBIA fibers present the highest elongation rate at break among the samples with different HrGO concentrations but the lower elongation rate at break than those of PBIA and 0.075-rGO/PBIA fibers (Figure S14a). Considering the size effect of reinforcement in composite fibers, HrGO with different lateral sizes were also investigated. As a result, the HrGO/PBIA fibers using HrGO with 1~2 μm lateral size present the higher tensile strength than those of composite fibers

using HrGO with ~5 μm and ~15 μm lateral sizes (Figure S14b). The HrGO with large lateral size inclines to aggregate, which will affect the polymerization of PBIA and lead to a reduced strength.

In some practical applications, PBIA fibers usually suffer from complex dynamic mechanical loading conditions, and thus the dynamic modulus of the fibers under different frequencies and strain rates effects were considered. Figure 4c displays the dynamic modulus of PBIA, 0.075-HrGO/PBIA, and 0.075-rGO/PBIA fibers under harmonic loads with different frequencies (20-200 Hz) during stretching processes[37], in which 0.075-HrGO/PBIA fibers display the higher modulus than those of PBIA and 0.075-rGO/PBIA fibers, implying that 0.075-HrGO/PBIA fibers would exhibit better antiseismic performance than PBIA fibers. In contrast to pure PBIA fiber, the dynamics modulus of HrGO/PBIA and rGO/PBIA fibers increase along with the frequency grows (Figure 4c). It is worth noting that the dynamic modulus of 0.075-rGO/PBIA is higher than that of PBIA fibers which is opposite to the quasi-static results in Figure 4b. According to the equation: $E = E' + iE''$, in which dynamic modulus E is synchronously related to the storage (E') and loss (E'') modulus. Therefore, the increase in dynamic modulus of 0.075-rGO/PBIA is resulted from the increase in loss modulus under the forced vibration. The strain rate effect is also crucial to evaluate the impact resistance of fibers. Figure 4d displays the modulus of PBIA, 0.075-HrGO/PBIA, and 0.075-rGO/PBIA fibers under different strain rates.[38] When the strain rates range from 1×10^{-5} to 5×10^{-3} s^{-1}, the initial modulus of these three kinds of fibers increases with the ascending strain rate. In addition, 0.075-HrGO/PBIA fibers present the higher initial modulus under different strain rates than PBIA and rGO/PBIA fibers, indicating that 0.075-HrGO/PBIA fibers exhibit an extraordinary shock-resistance when applied in real environment. In order to explore the cyclic-loading properties of HrGO/PBIA fibers, a series of cyclic loading experiments were conducted under a strain rate of 2×10^{-5} s^{-1}.[39] Initial strain of the fibers was set to 0.5%, and then an increment of 0.1% was exerted for each reloading cycle. According to the cyclic profiles of PBIA fibers (Figure 4e), residual strain is

observed in the 4th cycle and finally residual strain of PBIA fibers after 14 cycles is 0.75%. However, residual strain in 0.075-HrGO/PBIA fibers is hardly observed after 22nd cycles (Figure 4f). Moreover, the area crossed by the hysteresis loop at each cycle of 0.075-HrGO/PBIA is less than that of PBIA fibers (Figure S15), indicating that the internal interaction between molecules in the processes of cyclic stretching is strengthened because of the topological constraints between the HrGO and polymer chains. These results demonstrate that 0.075-HrGO/PBIA fibers exhibit a better stability than PBIA fibers under cyclic loadings.

Aforementioned experiments draw a conclusion that HrGO/PBIA composite fibers exhibit better comprehensive mechanical properties than PBIA and controlled rGO/PBIA fibers. The special holes on HrGO were considered to be the key role in improving mechanical properties of HrGO/PBIA fibers. The unique scaffolded structure in HrGO/PBIA fibers can effectively strengthen the lateral interaction of PBIA chains which run through the holes to form topological constrain structures. In order to further understand the enhancement mechanism, the molecular dynamics simulations using coarse-grained (CG) models were employed to demonstrate the structural evolution and interactions between HrGO and PBIA chains. Three CG models (PBIA, HrGO/PBIA, and rGO/PBIA composite fibers) were initially built with a cell size of 120×120×40 nm^3 (**Figure 5**a) and then relaxed to a dense state. In HrGO/PBIA model, the hole diameter of HrGO is about 1-2 nm and the concentration of HrGO is about 0.08 wt% which is close to the best experimental case. Before stretching (tensile strain $\varepsilon_z = 0$), molecular chains in HrGO/PBIA fibers are oriented along the axis with some deviations like that in PBIA fibers (Figure S16) and some PBIA chains run through the holes on HrGO. The HrGO sheets are not completely aligned to the axis, and some polymer chains penetrate the sheets serving as the topological constraints. As the strain increasing, topological constrains will prevent the chains from separating radially (Figure 5b). In contrast, the rGO sheets are nearly aligned to the axis in rGO/PBIA model (Figure 5c) and only interact with the chains by

the weak surface adhesion. The structure evolutions under stretching indicate that HrGO/PBIA presents stronger lateral interaction between PBIA chains via the topological constraints effect than rGO/PBIA. As a result, the HrGO/PBIA fibers exhibit the higher values of simulated tensile strength and modulus than those of PBIA and rGO/PBIA fibers (Figure 5d) which agrees with the experimental results. The typical simulated stress-strain profiles are shown in Figure S17. The tensile strength and modulus decrease along with the HrGO concentration further increase (Figure S18a), which is ascribed to the inferior aligned configuration of PBIA chains. Similar results were obtained in rGO/PBIA fibers (Figure S18b).

To better explain the performance improvement of HrGO/PBIA fibers, the von Mises shear strain distributions of these three typical models under stretching were calculated as shown in Figure S19-21. It is worth noting that the shear strain in the local region near HrGO exhibits obvious increase (Figure 5e) under stretching, which is not observed in rGO/PBIA model (Figure 5f), indicating the favorable structural relaxation by the chains sliding near HrGO. The local shear strain increase of HrGO/PBIA fibers are further demonstrated by the statistical shear strain distribution (Figure 5g), in which the local shear strain distribution is shifted to the higher value near HrGO but to the lower value near rGO, indicating that the PBIA chains bonding in HrGO exhibit stronger lateral interaction than that of PBIA or rGO/PBIA fibers. The increase of local shear strain logically leads to increase of global von Mises shear strain (Figure 5h) among whole fibers, then improving the final mechanical performance. Cycle-loading simulations were also conducted to theoretically probe the cyclability of HrGO/PBIA (Figure S22). The cyclic-loading simulations indicate that HrGO/PBIA fibers with different HrGO concentrations present a great improvement of modulus in the second stretching compared to that in the first stretching (Figure 5i). However, only a small modulus improvement is observed in PBIA model (HrGO = 0 wt% in Figure 5i). The cross-section structure of HrGO/PBIA and PBIA models after the first and second stretchings were also drawn and used to unveiled the reasons for modulus improvement (Figure 5j,k). Comparing with the structure of HrGO/PBIA

fibers after the first stretching, the micro-voids shrink and 3.7 % lateral size decline are observed in the second stretching structure of HrGO/PBIA fibers (Figure 5j), leading to a higher fiber density and stronger interaction between molecular chains in the presence of HrGO. Although the shrink of micro-voids and 3.4 % lateral size decline compared to structure after the first stretching are observed in the second stretching structure of PBIA fibers (Figure 5k), the higher voids density and relative weak lateral interaction lead to limited modulus improvement of PBIA fibers.

Conclusion

Novel scaffolded HrGO/PBIA fibers were prepared through *in-situ* polymerization method and controllable wet-spinning technology. Experimental results demonstrate that introducing HrGO into PBIA fibers significantly improves the mechanical properties PBIA fibers, in which 11.5% increasement in tensile strength and 8.3% increasement in Young's modulus are obtained with a concentration of HrGO about 0.075 wt%. Dynamic and cycle-loading measurements demonstrate the favorable compatibility of HrGO/PBIA fibers to actual application environment. CG model simulations were used to elucidate the enhancement mechanism and revealed that the reinforced strength and modulus are attributed to the holey structure of HrGO that can tightly bind the PBIA chains in the holes and strengthen the lateral interaction between polymer chains. This research not only expands the understanding of PBIA fibers but also provide a novel preparation method for graphene-reinforced composite fibers.

Experimental Section

Preparation of GO: GO was prepared by oxidation of natural graphite powder according to a room-temperature modified Hummers' method. Briefly, graphite (3 g) was added to concentrated sulfuric acid (70 mL) under vigorous stirring at 20 °C for 30 min. Then, potassium permanganate (9 g) was added slowly (over 2 h) into reaction system to avoid increasing the temperature of suspension. The oxidation process was conducted at 20 °C for 3 h. Successively, the reaction was terminated by pouring the resultant slurry into 1000 mL of icy deionized water.

As prepared graphite oxide sample was centrifugated at 1,000 g for 5 min. followed by being washed with 2000 mL HCl solution (1:10 v/v%) for 3 times and deionized water for 1 time by centrifugation. After that, graphite oxide dispersion was exfoliated by mild sonication at 20° C for 20 min, and further purified by dialysis for one weak. The resultant dispersion was subjected to 3 cycles of centrifugation at 1,000 g for 20 min to remove the graphite powder and unexfoliated graphite oxide agglomerates. Finally, the GO dilute dispersion was concentrated by centrifugation at 10,000 g for 1 h to obtain GO stock (solid content: 7 wt%).

Preparation of HrGO: HrGO was prepared according to the following procedures: 10 mL of 30% H_2O_2 aqueous solution was mixed with 100 mL of 2 mg mL^{-1} GO aqueous dispersion and then heated at 100 °C for 8 h under stirring. The as-prepared HrGO solution was purified by centrifuging and washed by deionized water to remove the residual H_2O_2. Then the HrGO solution was treated by freeze dryer to obtain HrGO powder with black color. The rGO powder was prepared under the same procedures in the absence of H_2O_2.

In-situ synthesis of PBIA and HrGO/PBIA spinning dope: The HrGO/PBIA composites fiber were prepared via a low temperature polycondensation, wet-spinning, and thermal treatment. Firstly, the optimized amount of HrGO was dispersed in DMAC, stirring and ultrasonication for 1 h, then the obtained homogenous HrGO/DMAC solution was slowly added in to the mixed solvent containing LiCl and DMAC, stirring for 40 minutes. And the whole *in-situ* polymerization reaction was conducted in a 10 L stainless steel reactor equipped with stirrer paddle. Subsequently, the polymerization of monomers consisting of PPD and PABZ were added into the above solution and stirring for 1 h. After cooling to below 10 ºC, TPC were added and stirred for 1.5 h. After the reaction completed, a black viscous polymer solution with a dynamic viscosity was obtained. As a control sample, the pure PBIA polymer solution was also obtained by a similar prepare procedure only without adding the HrGO powder. The dynamic viscosities of all these spinning dopes were controlled around 50000 cP.

Preparation of HrGO/PBIA fibers through wet-spinning: The obtained HrGO/PBIA polymer solution was poured into a degassing tank equipped with a metering pump and a nitrogen inlet. After a vacuum-defoaming treatment, the solution was transported to a spinneret plate consisting of 20 holes (The diameter of each hole is 0.1 mm), and injected into the primary coagulation bath of 50 wt% DMAC (50 wt% H_2O) and secondary coagulation bath of 20 wt% DMAc (80 wt% H_2O). The obtained primary fibers were obtained after washing and drying. Subsequently, the HrGO/PBIA fibers were obtained by a heating treatment in the N_2 atmosphere and collected via an automatic winding device.

Statistical Analysis: The FT-IR and TGA data are original data. XRD data are nomalized from original data. The average mechanical properties and corresponding standard deviations for each sample type were obtained based on ten measurement results, where the few sample strips that broke near the clamps were excluded from the calculations.

Supporting Information

Supporting Information is available from the Wiley Online Library or from the author.

Acknowledgements

J.L., Y.W., Z.X., and S.W. contributed equally to this work. This work was financially supported by the Ministry of Science and Technology of China (2016YFA0200100 and 2018YFA0703502), the National Natural Science Foundation of China (Grant Nos. 52021006, 51720105003, 21790052, 21974004, 5210020884 11890682, and 11832010), the Strategic Priority Research Program of CAS (XDB36030100), and the Beijing National Laboratory for Molecular Sciences (BNLMS-CXTD-202001).

Received: ((will be filled in by the editorial staff))
Revised: ((will be filled in by the editorial staff))
Published online: ((will be filled in by the editorial staff))

References

1. M. G. Dobb, D. J. Johnson, B. P. Saville, Compressional behaviour of Kevlar fibres. *Polymer* **1981,** *22*, 960-965.
2. L. Penn, F. Milanovich, Raman spectroscopy of Kevlar 49 fibre. *Polymer* **1979,** *20*, 31-36.
3. G. Lubin, S. J. Dastin, Aerospace applications of composites. In *Handbook of Composites*, Lubin, G., Ed. Springer US: Boston, MA, **1982**, 722-743.
4. Y. S. Lee, E. D. Wetzel, N. J. Wagner, The ballistic impact characteristics of Kevlar® woven fabrics impregnated with a colloidal shear thickening fluid. *J. Mater. Sci.* **2003,** *38*, 2825-2833.
5. T. J. Singh, S. Samanta, Characterization of Kevlar fiber and its composites: a review.

Mater. Today: Proceedings **2015,** *2*, 1381-1387.

6. L. Luo, Y. Wang, J. Huang, D. Hong, X. Wang, X. Liu, Pre-drawing induced evolution of phase, microstructure and property in para-aramid fibres containing benzimidazole moiety. *RSC Adv.* **2016,** *6*, 62695-62704.
7. L. Luo, Y. Wang, Y. Dai, Y. Yuan, C. Meng, Z. Cheng, X. Wang, X. Liu, The introduction of asymmetric heterocyclic units into poly(p-phenylene terephthalamide) and its effect on microstructure, interactions and properties. *J. Mater. Sci.* **2018,** *53*, 13291-13303.
8. R. Xu, Y. Qiu, S. Tang, C. Yang, Y. Dai, D. Zhang, Y. Gao, K. Gao, L. Luo, X. Liu, Preparation of high strength and toughness aramid fiber by introducing flexible asymmetric monomer to construct misplaced-nunchaku structure. *Macromol. Mater. Eng.* **2021,** *306*, 2000814.
9. C. Chen, X. Wang, F. Wang, T. Peng, Preparation and characterization of para-aramid fibers with the main chain containing heterocyclic units. *J. Macromol. Sci. Part B* **2019,** *59*, 90-99.
10. H. Avci, A. Hassanin, T. Hamouda, A. Kiliç, High performance fibers: a review on current state of art and future challenges. *J. Eng. Arch. Fac. Eskisehir Osmangazi University* **2019,** *27*, 85-92.
11. Y. Dai, C. Meng, S. Tang, J. Qin, X. Liu, Construction of dendritic structure by nano-SiO_2 derivate grafted with hyperbranched polyamide in aramid fiber to simultaneously improve its mechanical and compressive properties. *Eur. Poly. J.* **2019,** *119*, 367-375.
12. H. G. Chae, S. Kumar, Making strong fibers. *Science* **2008,** *319*, 908.
13. X. Ding, H. Kong, M. Qiao, Z. Hu, M. Yu, Study on Crystallization behaviors and properties of F-III fibers during hot drawing in supercritical carbon dioxide. *Polymers* **2019,** *11*, *856*.
14. X. M. Ding, H. J. Kong, M. M. Qiao, Z. F. Hu, M. H. Yu, Relationship between crystallization behavior and mechanical performance of F-III fibers under different

tensions in supercritical carbon dioxide. *Mater. Sci. Forum* **2020,** *976*, 77-83.

15. A. A. Leal, J. M. Deizel, J. W. Gillespie, Assessment of compressive properties of high performance organic fibers. *Compos. Sci. Technol.* **2007,** *67*, 2786-2794.
16. C. Yang, H. Wu, Y. Dai, S. Tang, L. Luo, X. Liu, Self-enhancement in aramid fiber by filling free hydrogen bonding interaction sites in macromolecular chains with its oligomer. *Polymer* **2019,** *180,* 121687.
17. K. Li, L. Luo, J. Huang, H. Wang, Y. Feng, X. Liu, Enhancing mechanical properties of aromatic polyamide fibers containing benzimidazole units via temporarily suppressing hydrogen bonding and crystallization. *J. Appl. Poly. Sci.* **2015,** *132*, 42482.
18. Y. Dai, Y. Han, Y. Yuan, C. Meng, Z. Cheng, L. Luo, J. Qin, X. Liu, Synthesis of heterocyclic aramid fiber based on solid-phase cross-linking of oligomers with reactive end group. *Macromol. Mater. Eng.* **2018,** *303,* 1800076.
19. L. Luo, Y. Yuan, Y. Dai, Z. Cheng, X. Wang, X. Liu, The novel high performance aramid fibers containing benzimidazole moieties and chloride substitutions. *Mater. Design* **2018,** *158*, 127-135.
20. Y. Dai, Y. Yuan, L. Luo, X. Liu, A facile strategy for fabricating aramid fiber with simultaneously high compressive strength and high interfacial shear strength through cross-linking promoted by oxygen. *Composites Part A: Appl. Sci. Manufact.* **2018,** *113*, 233-241.
21. W. Cui, D. R. King, Y. Huang, L. Chen, T. L. Sun, Y. Guo, Y. Saruwatari, C. Y. Hui, T. Kurokawa, J. P. Gong, Fiber-reinforced viscoelastomers show extraordinary crack resistance that exceeds metals. *Adv. Mater.* **2020,** *32*, 1907180.
22. A. D. Roberts, P. Kelly, J. Bain, J. J. Morrison, I. Wimpenny, M. Barrow, R. T. Woodward, M. Gresil, C. Blanford, S. Hay, J. J. Blaker, S. G. Yeates, N. S. Scrutton, Graphene-aramid nanocomposite fibres via superacid co-processing. *Chem. Commun.* **2019,** *55*, 11703-11706.

23. S. Stankovich, D. A. Dikin, G. H. Dommett, K. M. Kohlhaas, E. J. Zimney, E. A. Stach, R. D. Piner, S. T. Nguyen, R. S. Ruoff, Graphene-based composite materials. *Nature* **2006,** *442*, 282-6.

24. F. Meng, W. Lu, Q. Li, J. H. Byun, Y. Oh, T. W. Chou, Graphene-based fibers: a review. *Adv. Mater.* **2015,** *27*, 5113-31.

25. Z. Gao, J. Zhu, S. Rajabpour, K. Joshi, M. Kowalik, B. Croom, Y. Schwab, L. Zhang, C. Bumgardner, K. R. Brown, D. Burden, J. W. Klett, A. C. T. van Duin, L. V. Zhigilei, X. Li, Graphene reinforced carbon fibers. *Sci. Adv.* **2020,** *6*, eaaz4191.

26. Z. Xu, Gao C., In situ polymerization approach to graphene-reinforced Nylon-6 composites. *Macromolecules* **2010,** *43*, 6716-6723.

27. S. Ghobadi, S. Sadighikia, M. Papila, F. Ç. Cebeci, S. A. Gürsel, Graphene-reinforced poly(vinyl alcohol) electrospun fibers as building blocks for high performance nanocomposites. *RSC Adv.* **2015,** *5*, 85009-85018.

28. S. R. Kwon, J. Harris, T. Zhou, D. Loufakis, J. G. Boyd, J. L. Lutkenhaus, Mechanically strong graphene/aramid nanofiber composite electrodes for structural energy and power. *ACS Nano* **2017,** *11*, 6682-6690.

29. I. A. Kinloch, J. Suhr, J. Lou, R. J. Young, P. M. Ajayan, Composites with carbon nanotubes and graphene: An outlook. *Science* **2018,** *362*, 547.

30. X. Ding, Z. Zhang, H. Kong, M. Qiao, Z. Hu, L. Zhang, M. Yu, Influences of graphene oxide addition on mechanical properties of aramid fiber reinforced composites. *Mater. Express* **2019,** *9*, 578-586.

31. Y. Xu, C. Y. Chen, Z. Zhao, Z. Lin, C. Lee, X. Xu, C. Wang, Y. Huang, M. I. Shakir, X. Duan, Solution processable holey graphene oxide and its derived macrostructures for high-performance supercapacitors. *Nano Lett.* **2015,** *15*, 4605-4610.

32. B. Yang, L. Wang, M. Zhang, J. Luo, Z. Lu, X. Ding, Fabrication, applications, and prospects of aramid nanofiber. *Adv. Funct. Mater.* **2020,** *30,* 2000186.

33. Y. Shi, T. Qiu, X. Tuo, The bottom-up synthesis for aramid nanofibers: The influence of copolymerization. *J. Appl. Polymer Sci.* **2020**, e49589.

34. Z. Zhang; J. L. Yang; K. Friedrich, Creep resistant polymeric nanocomposites. *Polymer* **2004,** *45*, 3481-3485.

35. J. L. Yang; Z. Zhang; A. K. Schlarb; K. Friedrich, On the characterization of tensile creep resistance of polyamide 66 nanocomposites. Part I. Experimental results and general discussions. *Polymer* **2006,** *47*, 2791-2801.

36. G. Mittal, V. Dhand, K. Y. Rhee, S. J. Park, W. R. Lee, A review on carbon nanotubes and graphene as fillers in reinforced polymer nanocomposites. *J. Indust. Eng. Chem.* **2015,** *21*, 11-25.

37. J. Zhao, X. Zhang, Z. Pan, Q. Li, Wide-range tunable dynamic property of carbon-nanotube-based fibers. *Adv. Mater. Interfaces* **2015,** *2*, 1500093.

38. Y. Zhang, L. Zheng, G. Sun, Z. Zhan, K. Liao, Failure mechanisms of carbon nanotube fibers under different strain rates. *Carbon* **2012,** *50*, 2887-2893.

39. Z. J. Yang, Q. S. Yang, X. Liu, X. Q. He, K. M. Liew, Detailed investigation on elastoplastic deformation and failure of carbon nanotube fibers by monotonic and cyclic tensile experiments. *Carbon* **2015**, *94*, 73-78.

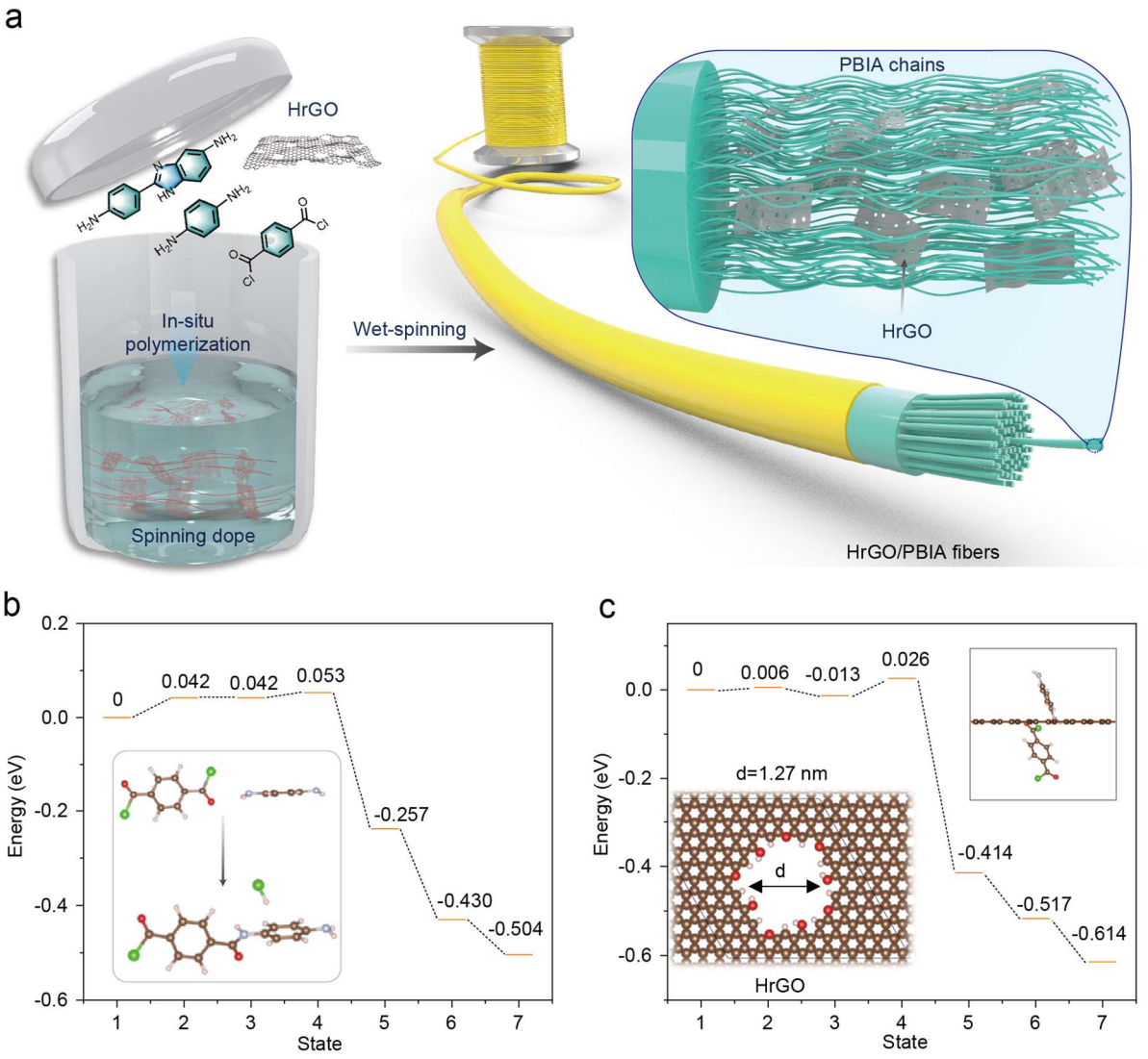

Figure 1. (a) Schematic diagram of in-situ polymerization processes of HrGO/PBIA composite fibers. Potential energy profiles of the polymerization of TPC and PPD in solution (b) and in the holes of HrGO (c). The insets in b are the reaction models of TPC and PPD. The insets in c are the models of HrGO (left) and adsorption configurations of TPC and PPD in the HrGO hole (right).

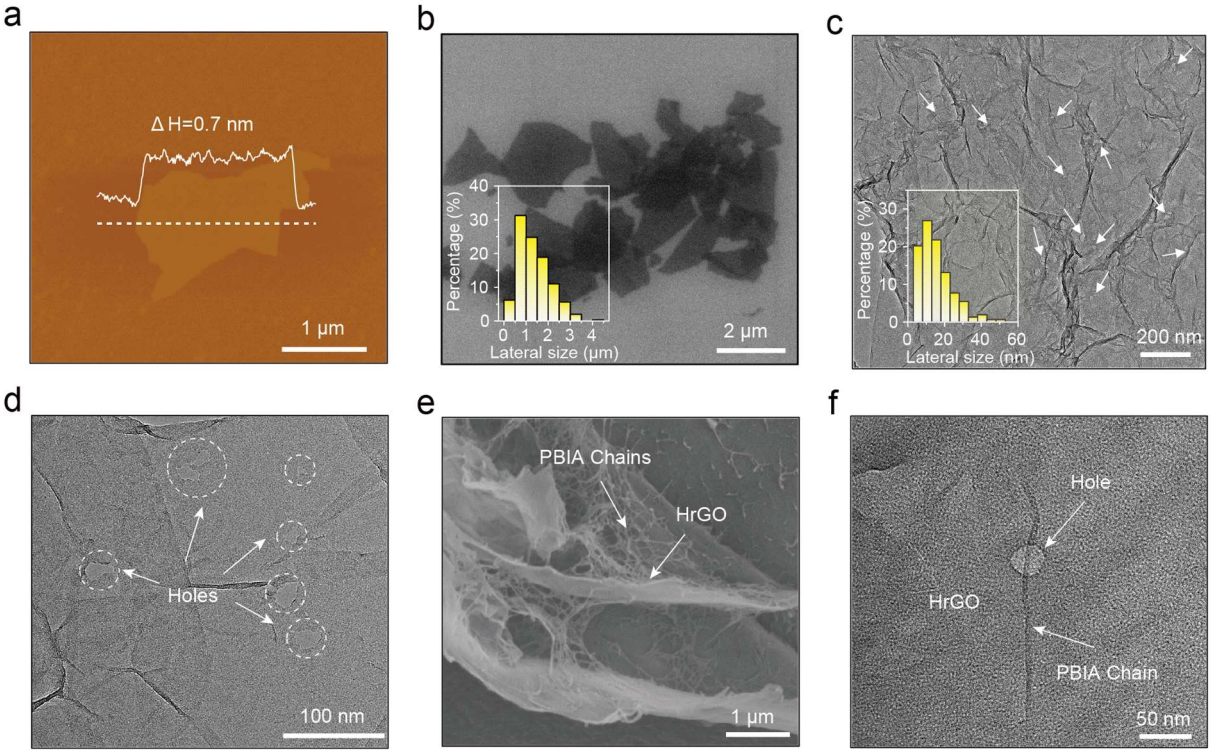

Figure 2. (a) AFM image of HrGO. (b) SEM image of HrGO. The inset is the histogram of the lateral size of HrGO. (c) TEM image of HrGO treated by H_2O_2 for 8h. The inset is the histogram of the lateral size of holes. (d) Zoom in TEM images of HrGO. SEM (e) and TEM (f) images of the composite structures of HrGO and PBIA polymer chains.

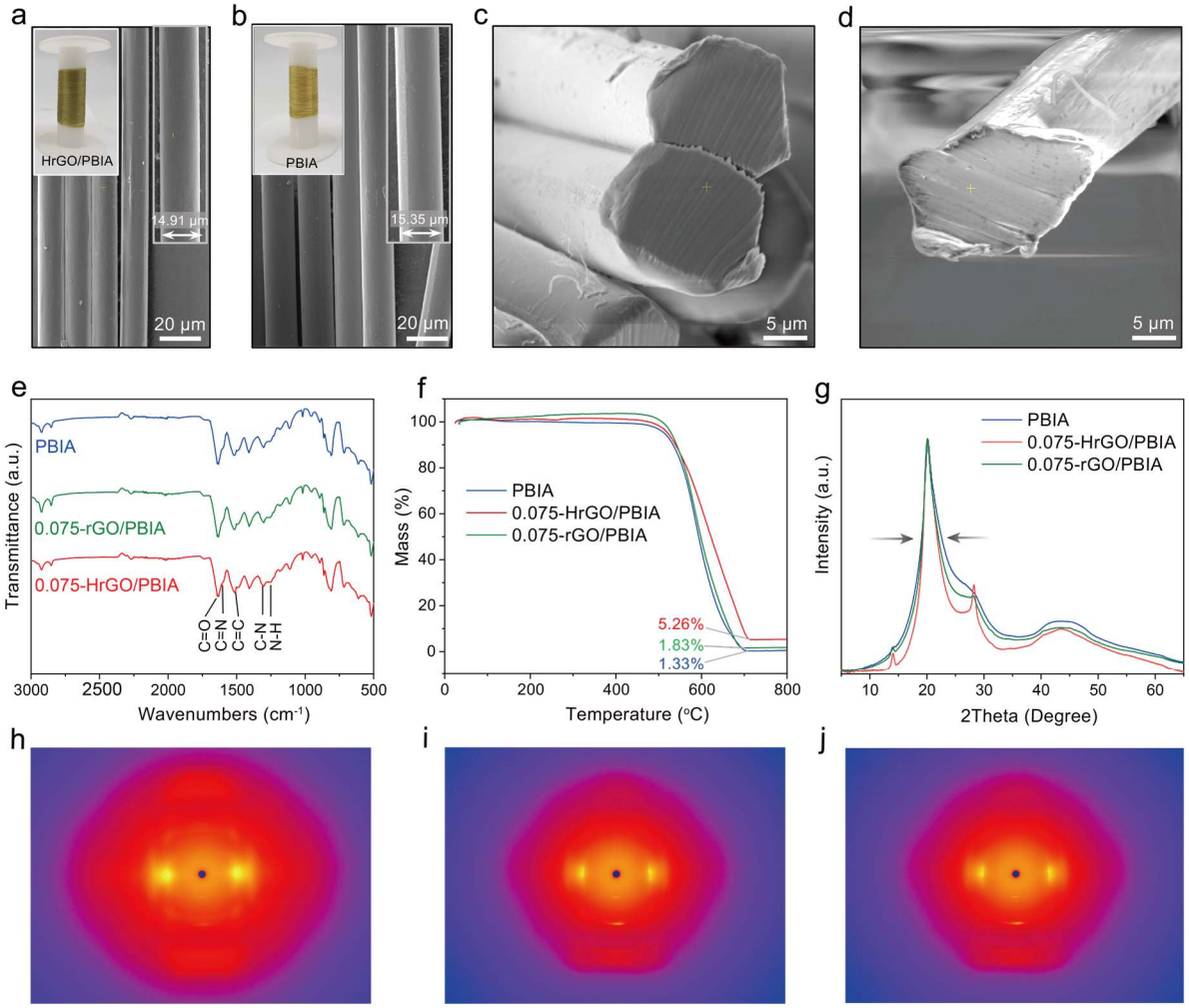

Figure 3. SEM images of 0.075-HrGO/PBIA fibers (a) and PBIA fibers (b). The left insets in a and b are the photography of HrGO/PBIA and PBIA fibers, respectively. The right insets in a and b are magnified SEM images of HrGO/PBIA and PBIA fibers, respectively. Cross-section SEM images of 0.075-HrGO/PBIA (c) and PBIA fibers (d). FT-IR spectra (e), TGA profiles (f), and 1D WAXS profiles (g) of PBIA, 0.075-HrGO/PBIA, and 0.075-rGO/PBIA fibers. 2D WAXS patterns of PBIA(h), 0.075-HrGO/PBIA (i), and 0.075-rGO/PBIA (j) fibers.

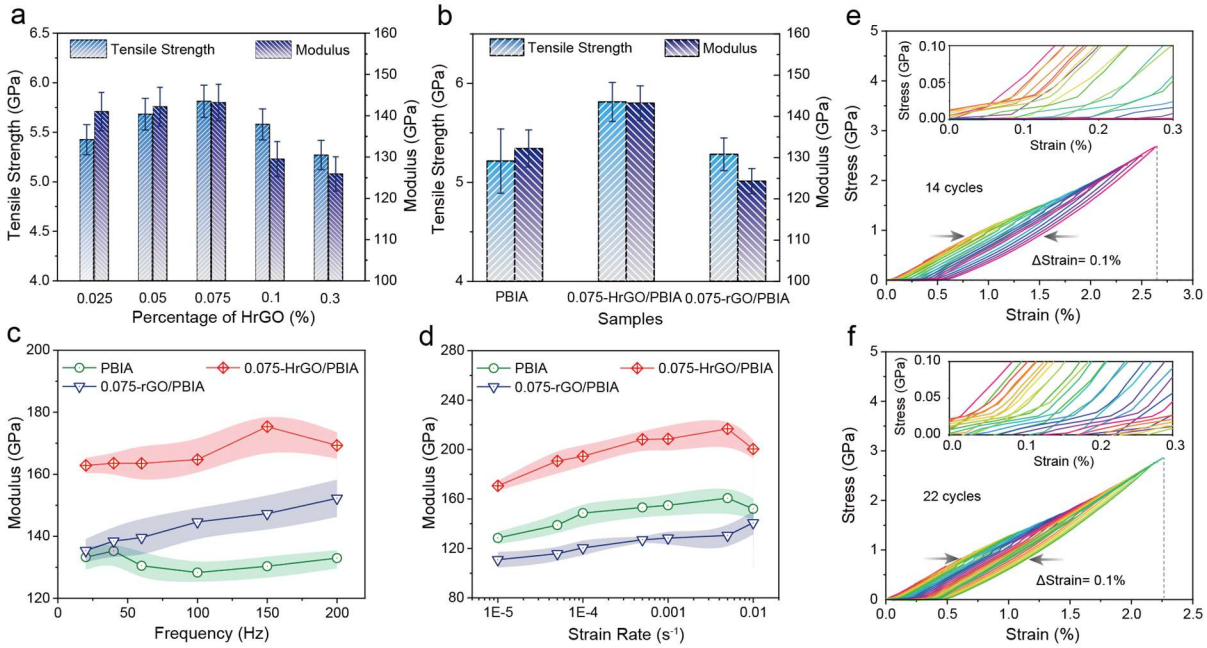

Figure 4. (a) Tensile strength and modulus of the HrGO/PBIA fibers with different HrGO concentrations. (b) Tensile strength and modulus of the PBIA, 0.075-HrGO/PBIA and 0.075-rGO/PBIA fibers. Dynamic modulus of PBIA, 0.075-HrGO/PBIA and 0.075-rGO/PBIA fibers under different loading frequencies (c) and different strain rates (d). Loading-unloading cyclic curves of PBIA (e) and 0.075-HrGO/PBIA (f) fibers.

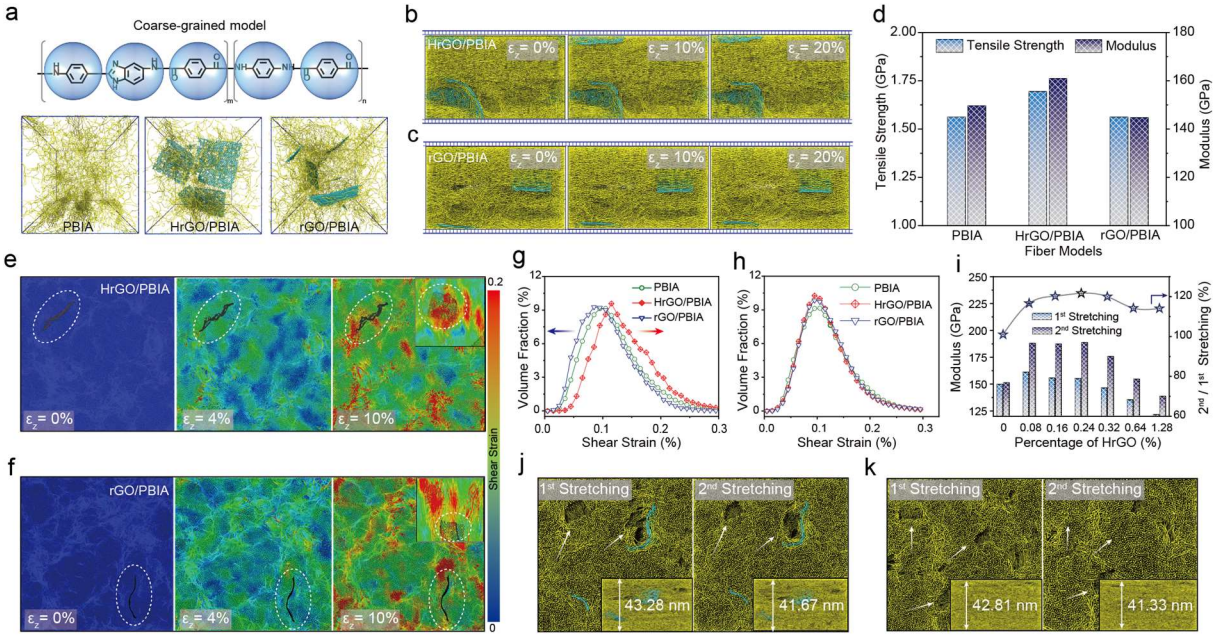

Figure 5. (a) Coarse-grained model of PBIA, HrGO/PBIA, and rGO/PBIA fibers. The cross-section models of HrGO/PBIA (b) and rGO/PBIA (c) fibers under different strains. (d) Theoretical strength and modulus of PBIA, HrGO/PBIA, and rGO/PBIA fibers. The von Mises shear strain distribution of HrGO/PBIA (e) and rGO/PBIA (f) fibers from cross-section view. The insets are the shear strain distribution from side view. Local (g) and global (h) von Mises shear strain distribution of PBIA, HrGO/PBIA and rGO/PBIA fibers. (i) Dynamic modulus of HrGO/PBIA fibers with cyclic-loading predictions. The cross-section and side-view geometric models of HrGO/PBIA (j) and PBIA (k) fibers after the 1st and 2nd stretchings.